Article Type: Research Articles

Catalytic degradation of O-cresol using H_2O_2 onto Algerian Clay-Na

Revised, 05 September 2018

Hayat Herbache[1], Amina Ramdani[1,2], Zoubida Taleb[1], Ramiro Ruiz-Rosas[3], Safia Taleb[1*]

Emilia Morallón[3], Laurence Pirault-Roy[4], Noreddine Ghaffour[5]

[1]*Laboratory of Materials & Catalysis, Faculty of Exact Sciences, Djillali Liabès university, BP 89, W-22000, Sidi Bel-Abbès, Algeria*

[2]*Department of Chemistry - Faculty of Sciences - University Dr. Moulay Tahar - Saida 20000 Algeria.*

[3]*Instituto Universitario de Materiales, Universidad de Alicante, Ap. 99. E-03080 Alicante, Spain.*

[4]*Institut de Chimie des Milieux et Matériaux de Poitiers, IC2MP UMR 7285, B27, TSA 51106, 4 rue Michel Brunet, 86073 Poitiers Cedex 9, France*

[5]*Water Desalination & Reuse Centre, King Abdullah University of Science and Technology (KAUST), Saudi Arabia*

ABSTRACT:

Clay material is used as a catalyst to degrade an organic pollutant. This study focused on the O-cresol oxidative degradation in aqueous solution by adding H_2O_2 and Mont-Na.

The catalytic tests showed a high catalytic activity of Mont-Na, which made it possible to achieve more than 84.6% conversion after 90 minutes of reaction time at 55 °C in 23.2 mM H_2O_2. The pH value was found to be negatively correlated with the degradation rate of O-cresol. UV-Vis spectrophotometry revealed that the increase of degradation rate at low pH is

related to the formation of 2-Methylbenzoquinone as intermediate product. In addition, the content of iron in Mont-Na decreased after the catalytic test, bringing further evidence about the O-cresol catalytic oxidation. The mineralization of O-cresol is also confirmed by the different methods of characterization of Mont-Na after the catalytic oxidation test. The effect of the O-cresol oxidation catalyzed by natural clay is significant.

KEYWORDS: O-cresol, Catalytic oxidation, Sodium clay, Hydrogen peroxide, Wastewater

Introduction

Environmental pollution from industrial and agricultural activities result in contaminated waters, posing significant health risks to living species (Gavrilescu et al., 2105; Hadjar et al., 2011). Therefore, the presence of the chemical pollution and in particular organic compounds, even in small quantities (doses), makes the water unsuitable for human consumption or even toxic (Tabué Youmbi et al., 2013; Shivaraman and Pandey, 2000). Cresols are industrial phenolic products, which can be found as water pollutants. They are colorless solids with a medicinal odor that can be liquid in the case of mixtures (ATSDR, 2008). There are three forms of cresols that differ slightly in their chemical structure: Ortho-cresol (O-cresol), meta-cresol (m-cresol), and para-cresol (p-cresol). These forms are presented separately or as a mixture (Vijayakumar et al., 2011). They are produced or utilized in oil refineries, pharmaceutical industry, agribusiness and in household disinfectants (William and Roper, 1992; Yi et al., 2008). Under the environmental protection laws, several countries have recognized cresols as very toxic phenolic micro-pollutants by either contact, inhalation or ingestion, causing serious health and environmental problems (Chena et al., 2016). They appear in several lists of priority hazardous substances, such as those published by the Agency for the Registry of Toxic Substances and Diseases (ATSDR) and the United States Environmental Protection Agency (USEPA) (Lassouane et al., 2013). In addition, the

USEPA sets a regulatory framework, which considers cresols as persistent and priority toxic products and show that limit values should not exceed 12 µg/L (Kavitha and Palanivelu, 2005; Shadnia and Wright, 2008). Their allowable mass content in industrial wastewater is not listed in the Algerian regulations. However, that of phenol is published: it must not exceed 1 mg/L in the discharge of wastewater treatment plants and 2 µg/L in treated wastewater used for irrigation purposes (Official Journal of the Algerian Republic N°41, 2012).

Current purification techniques are able to remove most pollutants satisfactorily, but these techniques often have a high cost. Methods for the removal of o-cresol can be classified into two groups: i) non-destructive methods: coagulation, chemical precipitation, ion exchange, adsorption, ion exchange resins (Wang et al., 2015; Kennedy et al., 2005; Toh et al., 2013; Huang, 2009; Titus et al., 2002; Li et al., 2018) and membrane processes (Jiang et al., 2015; Wernert et al., 2015). (ii) Destructive methods: chemical oxidation, electrochemical oxidation and photocatalytic oxidation (Shahrezaei et al., 2012; Khunphonoi and Grisdanurak, 2016; Borji et al., 2014; Ling et al., 2015) and biological treatment (Adav et al., 2007; Ren et al., 2014). Chemical oxidation presents itself as a technology of choice for the treatment of wastewater, because it is an efficient, simple and economical process. It can replace biological processes when they are not effective enough (Zaviska et al., 2009). Moreover, the adsorption treatment is the technique of choice for the reduction of organic micro-pollutants.

Several studies have shown that adsorption on clay is easily achievable (Kausar et al., 2017; Ramdani et al., 2015; Sennour et al., 2009; Feddal, et al., 2014; Hocine et al., 2004), and the combination of both adsorption and chemical oxidation processes has also shown a huge capacity for the abatement of wastewater pollutants, which are not biodegradable, have toxic character and / or present high concentrations (Hernandez-Esparza et al., 2010; Khaki

et al., 2017; Salazar-Gil et al., 2017). In this sense, the catalytic properties of clay for several reactions with industrial applications (hydrogenation, oxidation and polymerization) were highlighted several decades ago (Bertella et al., 2015; Saiah et al., 2017). Bridged clays have been studied as a catalyst to remove organic pollutants in the presence of H_2O_2 (Kurian and Sugunan, 2006; Molina et al., 2006; Ellias and Sugunan, 2014; Gil et al., 2008). Ammonia, nitrates, dinitrogen, halides and/or sulfur can be also obtained if nitrogen, sulfur and/or halogens are found in the formulation of the pollutants (Deng and Englehardt, 2006; Yan et al., 2016). The oxidation processes in the liquid phase in the presence of H_2O_2 are known to be highly effective. In the presence of certain metal ions, and more particularly Fe (II), the formation of hydroxyl radicals (OH •) or hydroperoxide (HOO•) takes part leading to the catalytic oxidation of cresol (Zaviska et al., 2009; Deng and Englehardt, 2006; Yan et al., 2016; Adan et al., 2009). It is important to emphasize that the use of this oxidant alone is not effective for most organic products (Lahbabi et al., 2009). Oxidation processes consist in partial or total oxidation to form inorganic by-products, carbon dioxide and water, which are safe and non-toxic to the environment (Zaviska et al., 2009; Navalon et al., 2010).

Several authors have studied the use of the oxidation processes for the removal of organic pollutants. Thus, ~~Ying~~ Yan et al (2016) performed a wet catalytic oxidation of phenol using a Fe_2O_3 (Fe_2O_3/ MCM-41) doped zeolite suspension in a fixed bed reactor. The influence of the reaction temperature, the height of the catalyst bed and the feed rate was optimized. Then, the mechanism of reaction of the wet catalytic oxidation of phenol on Fe_2O_3/MCM-41 was studied by determining the concentrations of intermediates. The results showed that the conversion rates of phenol, H_2O_2 and TOC reached 99%, 91%, and 72.5%, respectively under optimum operating conditions (feed rate of 2.0 ml / min, temperature 80 °C and catalyst bed height of 4 cm). Phenol is converted to benzoquinone, catechol and hydroquinone.

Kurian and Sugunan (2006) studied the Wet Peroxide Oxidation (WPO) using as catalyst pillared clays with Fe/Al in the presence of H_2O_2. The results showed a maximum oxidation of phenol of 78%, reached at 15 min and 80 °C: In addition, it was demonstrated that there is a synergistic effect between these metals. A mechanism involving the formation of phenoxy radicals on the surface of the catalyst, which then reacts with the peroxide to give OH radical and di-phenol. The produced free radical propagates the chain by attacking the phenol molecule, forming di-phenols.

In a different work, four types of activated carbon catalysts derived from coconut (SAC), coal tar (PAC), coal (CAC) and oak wood (WAC) were used in the CWPO process for the catalytic oxidation of m-cresol in waste water in the presence of H_2O_2 (Wang et al., 2015). The higher catalytic activity of crude activated carbons is the result of their active sites which are rich in structural electrons at their surfaces, which could improve the efficiency of H_2O_2 to more than 95%. The Fe added to the carbon catalyst could also produce that total carbon content (TOC) removal and m-cresol conversion reached a 30% and 95%, respectively, after 2000 h in a chemical wet peroxide oxidation (CWPO) process. The Fe/SAC catalyzed reaction also revealed a conversion rate of 90% m-cresol in 1800 hours. 2-methyl-p-benzoquinone and short-chain carboxylic acids were considered to be the major products in this catalytic oxidation of m-cresol, which were detected by gas chromatography-mass spectrometry and then calculated by density functional theory.

This study evaluates the oxidative elimination of o-cresol in aqueous solution using local sodium clay (Mont-Na), in the presence of hydrogen peroxide H_2O_2 at moderate temperatures. Here we attempt to show how the introduction of the hydrogen peroxide reagent on O-cresol supported by the clay modifies the properties of the latter, in particular its

adsorption capacity in its oxidation capacity. The catalyst was characterized before and after oxidation by X-ray diffraction, X-ray fluorescence, Fourier transform infrared spectroscopy, N_2 adsorption-desorption isotherm, chemical composition, pH at point of zero charge and thermogravimetry coupled to mass spectroscopy (TGA / DTA-MS).

Methodology

Experimental protocol

Aqueous solutions of O-cresol were prepared by dissolving a known mass of o-cresol with deionized water in volumetric flasks. The stock solutions were stored in the dark at room temperature and then diluted to the desired concentrations. The oxidation experiments were conducted in batch mode using a multi-station stirrer device (Memmert IPP200-500, 9 stations) with thermostatic bath (temperature controlled) with a regulated horizontal oscillation (300 cps/min). In a typical experiment, 15 mg of Mont-Na (Commercial sodium clay of Montmorillonite type (Mont-Na) is provided by ENOF Company, National Company of the Non-ferrous Mining Products, Algeria) is suspended in a volume of 250 mL of a solution of O-cresol (62.5 mg/L) and H_2O_2 (23.3 mM) (Herbache et al., 2016). However, different H_2O_2 concentrations have been studied and an experiment without clay was also analysed. The contact time is modified from 0 to 135 min. After such time, the liquid phase is recovered and filtered, and the concentration of O-cresol in aqueous phase was determined by UV-VIS at λmax = 270 nm. The presence of different intermediates has been elucidated using also UV-VIS. The pH of this eluate is measured using CRISON micro pH 2001 device. The main parameters determined during the catalytic tests are thus pH, the O-cresol concentrations, intermediates and in H_2O_2. The experimental tests of o-cresol adsorption over Mont-Na were carried out in previous work (Herbache et al., 2016). The conversion of O-cresol is calculated using the following equation:

$$\% \text{ Conversion} = \frac{(C_i - C_{eq})100}{C_i}$$

where Ci is the initial concentration of O-cresol (mg/ L), Ceq is its equilibrium concentration, which is determined at the end of the selected contact time (mg/L).

Characterization of the catalyst (Mont-Na)

X-ray fluorescence (XRF)

X-Ray Fluorescence analysis (XRF) measurements of the elemental compositions of catalyst (clay) before and after oxidation were obtained using an automatic sequential wavelength dispersive X-ray fluorescence spectrometer PW 2400 (Philips). Around 100 mg of samples were employed in order to deliver representative results.

X-ray diffraction (XRD)

The X-ray diffraction analyzes of the samples were made using a Bruker D8-Advance diffractometer operating at the copper Kα wavelength (λ = 1.5406) at a voltage of 20-60 kV and an intensity of 5-80 mA.

FT- infrared spectroscopy

Fourier transform infrared spectroscopy (FTIR) was performed using a Bruker Alpha Model Frontier/Multiscope spectrophotometer over a range of 350 to 3800 cm^{-1} with a resolution of 2 cm^{-1}.

Thermogravimetric analysis coupled with mass spectrometry:

Temperature programmed desorption (TPD) experiments were performed in a TG-TDA equipment (Mettler Toledo, TGA/SDTA851e/LF/1600) coupled to a mass spectrometer (Pfeiffer Vacuum, THERMOSTAR GSD301T). The thermobalance was purged for 2 h using

a helium flow rate of 100 ml min-1 before the TPD running, and then heated up to 950 ºC (heating rate 20 ºC min^{-1}) while keeping the inert atmosphere.

Specific surface (S_{BET}) and point of zero charge pHpzc

The specific surface area of the adsorbents was determined by nitrogen physisorption at 77 K, using a Micromeritics ASAP 2000 volumetric adsorption device. The specific surfaces (S_{BET}) of the adsorbent before and after adsorption and in the presence or absence of H_2O_2 were calculated using the BET (Brunauer-Emmett-Teller) equation assuming that the surface of the nitrogen molecule is 16.2 $Å^2$. The microporous volumes and the pore width are calculated by applying the methods of Dubinin-Radushkevich (DR) and Barrett, Joyner and Halenda (BJH) to the N_2 adsorption-desorption isotherms. The point of zero charges pH_{PZC} has been estimated according to previous work (Herbache et al., 2016).

UV-Visible spectrophotometry

The concentration of targeted compounds during the catalytic oxidation kinetic tests were followed by UV-Visible spectrophotometry using a brand Perkin-Elmer spectrophotometer (model Lamda 45) dual beam, operating over a range of 190 to 1100 nm. The wavelength of the absorption maxima of O-Cresol is λ_{max} = 270 nm and that of 2-Methylbenzoquinone λ_{max} = 250 nm.

Results and discussion

Effect of H_2O_2 addition

In order to determine the effect of H_2O_2 reagent addition on catalytic oxidation, tests were carried out in the presence of the catalyst at different concentrations of H_2O_2 at a temperature of 25 °C.

Figure 1.

The results compiled in Fig. 1 show that the conversion of O-cresol decreases with H_2O_2 concentration. Therefore, the maximum removal of the pollutant was achieved at the lowest H_2O_2 concentration, 23.2 mM, where the oxidation yield of O-cresol was 73.6%. This hydrogen peroxide concentration has been fixed for the remaining oxidation tests. This correlates well with the results obtained from previous studies (Yan et al., 2016, Ling et al., 2015; Navalon et al., 2010), who studied in their works that adding H_2O_2 promoted catalytic oxidation process, the degradation rate of phenolic compounds was obviously increased and involves the generation and subsequent reaction of hydroxyl radicals ($OH^{\bullet}$). Maximum degradation efficiency was attained at 31.64 mM for all the cresol isomers studied. Moreover, addition of peroxide hydrogen, did not affect the degradation efficiency, this due to self-decomposition of H_2O_2 (Kavitha and Palanivelu, 2005).

Effect of temperature

Figure 2 shows that the temperature has a major effect on the process of oxidation. It clearly increases the degradation of the pollutant owing to the decomposition of hydrogen peroxide in presence of catalyst into free radicals (Kavitha and Palanivelu, 2005; Zaviska et al., 2009; Khaki et al., 2017; Yan et al., 2016). In order to observe more clearly the effect of temperature, the conversion of O-cresol for a fixed time has been compared at different temperatures, Figure 2. Indeed, when the temperature of the reaction increases from 25 °C to 55 °C, the conversion rate of O-cresol increases from 73.6% to 84.6%. Similar findings are reported by different authors (Kurian and Sugunan, 2006; Lahbabi et al., 2009).

Figure 2.

Effect of contact time

The kinetics of the catalytic oxidation of O-cresol with H_2O_2 in the presence of clay has been analyzed in order to determine the time required for achieving the maximum oxidation. For this purpose, the conversion of O-cresol was monitored at different temperatures (25°, 35°, 45° and 55°) with time. Figure 3 shows the conversion of O-cresol as a function of the reaction time. In the absence of catalyst, blank experiments indicated the absence of any significant degradation of O-cresol. Contrarily, the presence of Mont-Na greatly increases the conversion of the phenol compound. Thus, the catalytic oxidation process achieves O-cresol high conversions of more than 50% even 70% at 25 ºC and 55 ºC, respectively. Beyond this time, the conversion rate of o-cresol remains constant. From the curves obtained, the reaction time required for degradation of O-cresol to reach equilibrium of 84% at 55 °C and 73% at different temperatures is up to 90 and 120 min, respectively. It has been shown in many researches that time has a promotional effect on the degradation of phenolic compounds. The catalytic performances of iron aluminium mixed pillared Montmorillonite and mesoporous material Fe_2O_3 /MCM-41 towards hydroxylation of phenol with H_2O_2 (Kurian and Sugunan, 2006; Yan et al., 2016).

Figure 3.

Effect of pH

From the results of figure 4, it has been found that the degraded amount of O-cresol is greater and favored in a strongly acidic medium pH = 2 for all temperatures studied. It gradually decreased when the solution became neutral and basic Figure 4.

These results can be interpreted as follows:

i) On the one hand, the oxidation depends on the nature of charges of the catalyst sites and the behavior of the oxidant H_2O_2 according to the pH_{pzc} value of Mont-Na, which is = 5.11. At pH below pH_{pzc} (pH = 2), catalytic oxidation is favored by increasing the number of positive charges of the reactive (H^+) sites of the catalyst (clay) that react with the oxidant H_2O_2/Fe^{2+} contained in the Mont-Na to produce free radicals ($HO^\bullet$) in situ.

ii) On the other hand, at $pH_{pzc} > 5.11$ and therefore at neutral and basic pH (7 and 10), there would be an increase in the number of negative charges of active sites (OH^-). Thus, the surface of Mont-Na becomes negatively charged, and consequently, the conversion rate of O-cresol decreases probably due to the electrostatic interaction of Fe^{2+} with OH^-. Moreover, the redox potential of H_2O_2 decreases when the pH increases.

Indeed, it is shown in the literature that the decomposition of hydrogen peroxide (H_2O_2) by iron generates radical species ($HO^\bullet$) that are highly reactive with respect to organic molecules. This reaction is called the Fenton process. The catalytic oxidation reactions and in particular the decomposition of H_2O_2 by the ferrous ions are presented as follows (Kavitha and Palanivelu, 2005; Wang et al., 2015; Zaviska et al., 2009):

$$H_2O_2 + Fe^{2+} \longrightarrow OH^\bullet + OH^- + Fe^{3+} \quad (1)$$

$$RH\ (pollutant) + OH^\bullet \longrightarrow (R^\bullet) + H_2O \quad (2)$$

$$(R^\bullet) + H_2O_2 \longrightarrow ROH + OH^\bullet \quad (3)$$

In a very acidic medium (pH = 2) this mechanism is favored by the increase of the H_2O_2/Fe^{2+} ratio (Zaviska et al., 2009). On the other hand, at neutral and basic pH, iron (Fe^{2+} and Fe^{3+}) is able to precipitate and form iron hydroxides, thus leading to a slight decrease in catalytic activity (Kavitha and Palanivelu, 2005; Wang et al., 2015; Zaviska et al., 2009; Kurian and Sugunan, 2006; Molina et al., 2006; Ellias and Sugunan, 2014). Our results seem

to be in agreement with this mechanism. In fact, in Table 1, the reduction of the iron content after the catalytic oxidation shows that the oxidation process has taken place. This correlates well with the results interpreted previously.

The free radicals $OH^{\bullet}$ have a very marked electrophilic character, and organic compounds with electron donor groups react more rapidly with them, leading to the formation of ortho or para-hydroxylated intermediates via an electrophilic reaction (Zaviska et al., 2009). Several studies have been made for the catalytic oxidation of phenol and cresols (Wang et al., 2015; Khunphonoi and Grisdanurak, 2016; Zaviska et al., 2009; Adan et al., 2009; Valsania et al., 2012), and have allowed to identify the formation of pyrocathecol, hydroquinone and benzoquinone. Indeed, the degradation of O-cresol in by-products is similar to that of phenol. The di-hydroxylated products (biphenols) are in turn attacked by the free radicals $OH^{\bullet}$ leading to the opening of the aromatic ring, forming carboxylic acids and finally the H_2O and CO_2.

Figure 5.

Figure 6.

Also, the representation of the absorbance of the disappearance of O-cresol (λ_{max} = 270 nm) as a function of time (Figure 5) confirms these results. In it, the by-product formation is observed: 2-methylbenzoquinone (λ_{max} = 250 nm) following degradation of O-cresol. A yield of more than 84.6% degradation of o-cresol is obtained after 80 minutes of reaction time at a temperature of 55 °C. The final absorbance values of cresol and 2-methylbenzoquinone decrease considerably. These results show that O-cresol is completely degraded and that 2-methylbenzoquinone is transformed into other by-products.

Figure 6 shows the evolution of the pH of the medium during the oxidation of O-cresol. The rapid pH decrease from 6.4 to 4.5 proves that there is formation of 2-methylbenzoquinone and methylhydroquinone after 5 min of oxidation. Indeed, hydroquinones and benzoquinones are di-acids whose pH is between 4 and 4.7. The next oxidation step is the opening of the benzene ring, leading to the formation of carboxylic acids, which justifies the low pH values observed after 5 minutes (Fig. 6). After such time, the pH value increases and reaches a neutral value after 60 min of oxidation. This would be a proof that the carboxylic acids are being degraded to H_2O and CO_2 in the later stages of the treatment. Figure 7 presents a possible degradation scheme for the O-cresol oxidation process taking place in the presence of Mont-Na (Figures 6 and 7).

Figure 7.

There have been numerous references in the literature to investigate the cresol degradation mechanism by other oxidation process: ozonation, electrochemical oxidation and photocatalytic oxidation etc…Several highly hydrophilic degradation intermediates have been identified (Valsania et al., 2012) for cresols. The ozonation reaction mechanism assumed is subdivided into 3 steps, involving the ring opening of the phenolic group, followed by the formation of several by products intermediates in the increasing oxidation state. This leads subsequently to the formation of relatively stable products, such as carboxylic acids (malonic and oxalic). The electrochemical behaviour of cresol on platinum electrodes has been studied using cyclic voltammetry and in situ FTIR spectroscopy (Taleb et al., 2014). From the results, it can be concluded that the main soluble products formed during the oxidation of O-cresol in acid medium are CO_2 and methyl-p-benzoquinone.

Abdollahi et al., 2011 studied the degradation of o-cresol in the presence of UV; by ZnO as photocatalyst. The results showed that the photodegradation of O-cresol leads to the formation of the intermediates: 2- methylresorcinol, 2.5-hydroxybenzaldehyde, and may be the presence of carboxylic acids.

X-ray fluorescence

Table 1 shows the XRF analysis of the Mont-Na before and after the catalytic oxidation. The analysis has been repeated again on a sample recovered after the catalytic oxidation test at 55 ºC. The presence of oxygen (O) and silicon (Si) in a substantial amount, and of aluminum (Al) and iron (Fe) in a lower extend, is expected owing to the well-known composition of Mont-Na. After the catalytic tests are completed, it can be seen that Fe and Al levels are lowered from 2.04 to 1.62% and 12.5 to 9.85 %, respectively. Also, an observed increase of O content from 48.9 to 49.6%.

The quantitative elemental analysis of Mont-Na catalysts have been performed by means of X-ray fluorescence and the results are presented in Table 1.

Table 1÷

It can be observed that the clay contains a high amount of iron that could participate in the mechanism of oxidation of O-cresol. Then, the introduction of H_2O_2 could improve the oxidation of this compound by the formation of radicals as the well-known Fenton mechanism, because in the absence of clay any significant degradation of O-cresol is produced.

X-ray diffraction (XRD)

X-ray diffraction was performed for three samples: Mont-Na local clay before and after adsorption (Mont-A) and also after catalytic oxidation of O-cresol (Mont-AO). The initial XRD profile shows the lines corresponding to Montmorillonite and Illite. Examination of the local Mont-Na clay diffractogram (Figure 8) indicates a lattice distance of 12.6 Å. It should be noted that both the adsorption and the catalytic oxidation of O-cresol have undergone significant changes in Mont-Na structure, as pointed out by the slight decrease in the intensity of the signal collected and the shifting of the characteristic peaks of Montmorillonite. The diffractogram of Mont-A shows an increase of d_{001} from 12.6 to 14.5 Å. This variation is due to the presence of O-cresol molecules incorporated in the interfoliar space during adsorption. The diffractogram of the local clay in the presence of the oxidant H_2O_2 shows an increase in the basal area of the Mont-Na sample. Thus, the peak at 12.6 Å of the (001) sample line (Mont-OA) widens and reaches a maximum of 15.2 Å over that of the Mont-A sample. This is due to the hydration of the catalyst by the water molecules formed during the oxidation to more than 84% cresol, the rest being incorporated into the interfoliar space. In addition, the height of all Montmorillonite peaks of decreases (2θ = 20.6 °, 21.5°, 23.1°, 27°, 43º). The height of all the Illite peaks decreases (2θ = 14.90°, 20.70° and 29.36°).

Figure 8.

Infrared spectroscopy

Changes in the surface chemistry of Mont-Na after adsorption and oxidation experiments have been analyzed by means of FTIR, being reported in Fig. 9. The disappearance of certain bands in the spectra of the samples is noted. This is the case for Mont-A and Mont-AO samples, where the peak located at 1464 cm^{-1} in Mont-Na, characteristic of carbonates, is no longer seen, pointing out the disappearance of impurities (Herbache et al., 2016; Madejova,

2003). The band located between 3200 and 3750 cm^{-1}, with a shoulder at 3622 cm^{-1} characterizing Montmorillonite, corresponds to the elongation vibrations of the OH groups of the octahedral layer (Madejova, 2003). As for the OH bands, the comparison between the three spectra reveals a decrease and an increase are recorded in the intensity of stretching vibration bands of OH groups. They are centered at 1634 cm-1 , for the Mont-A and Mont-AO samples following the catalytic oxidation of O-cresol, respectively. They are also associated to the OH groups of the water constitution and the water adsorbed between the sheets. In addition, a large observed widening of the band corresponds to the elongation vibrations of the OH groups of the octahedral layer for Mont-OA situated around 3200 -3750 cm^{-1}.

Figure 9.

Textural properties

The porosity of Mont-Na has been determined from the N_2 adsorption-desorption isotherms before and after the O-cresol adsorption and oxidation experiments. Table 2 compiles the most important textural parameters that are calculated from the N_2 adsorption isotherms. Mont-Na shows a type IV porous isotherm, characteristic of mesoporous solids. Surface area as determined from BET method starts at 67 m^2/g for Mont-Na. This value decreases to 43 m^2/g after adsorption of O-cresol (Mont-A sample in Table 1). This is related to the existence of O-cresol molecules inserted into the interlaminar space. Interestingly, the reduction of the specific surface area is even larger for the Mont-AO sample (40 m^2/g) when compared to the surface of the Mont-A sample. However, the micropore volume increases after the adsorption and oxidation experiments, Table 2. This can be related to the removal of impurities, such as carbonates, which have been already documented in the FTIR results.

Table 2.

Thermogravimetric analysis coupled with mass spectrometry

Three (03) stages of dehydration (elimination of water), endothermic process characterizes the sodium clay: Mont-Na, Figure 10. The first step corresponds to the removal of hygroscopic water (starting water molecules free of hydration) at a temperature <100 °C. The second corresponds to the loss of weight associated with the desorption of the water adsorbed in the interfoliar space at a temperature of 450 °C. The last step corresponds to the elimination of the water constitution of the clay (dehydroxylation of the sheets (OH^- of the structure of clays (crystalline water) at the temperature of 600 °C.

So, the weight loss is 2.5% of free water molecules of hydration between 50 and 90 °C. 2.0% for the water adsorbed in the interfoliar space at 400 °C. Finally, the loss in weight is 13% for the water associated with the dehydroxylation of the sheets (crystalline water) (Mohan and Pittman, 2007; Ourari et al., 2018), towards 600 °C.

Figure 10.

In Figure 11, the thermogravimetric profile of O-cresol/Mont-Na adsorption has four endothermic stages, three of which correspond to the desorption of the three different types of water discussed above and whose quantities have changed. 7.5% of free water molecules of hydration are desorbed in the first step. Between 100 and 150 °C, the desorption of O-cresol is 13%. A loss in weight of 2.0% of the water adsorbed in the interfoliar space at 400 ° C and a loss in weight of 4% of the water associated with the dehydroxylation of the sheets (OH^- of the structure of the clays (Mohan and Pittman, 2007), towards 600 °C.

Figure 11.

For the oxidation of O-cresol-Mont-Na, Figure 12, there is also four endothermic stages, three of which correspond to the loss of the three different types of water discussed above and whose quantities have changed. The weight of the remaining O-cresol is 4%, and weight loss of free water molecules and the water of the interfoliar space is 13% and 0.5%,

respectively. Finally, a loss in weight of 4% of the crystalline water (Mohan and Pittman, 2007), towards 600 °C is observed.

Figure 12.

It is important to note that the amount of desorbed water has increased during the oxidation reaction. Indeed, the mass loss (Figure 12) is 13% relative to the 7.5% mass loss (Figure. 11) during the adsorption of cresol in the absence of H_2O_2. This could confirm the total oxidation of the pollutant by forming H_2O and CO_2. In addition, the DTA coupled to the MS allow us to confirm this degradation since in Figure13, under the atmosphere of inert gas (Helium), the presence of CO_2 and H_2O is noted. The presence of CO_2 would come from the decomposition of cresol. Mass Spectroscopy does not detect the latter.

Figure 13.

It should be noted that the peak of CO_2 is more intense under atmospheric air because of the presence of this gas in the air (Figure 13).

Conclusions

In this work, the use of local clay shows a great potential for catalyst properties in the presence of the oxidizing reagent H_2O_2 for the degradation of O-cresol. The effect of some experimental parameters has been studied using a batch oxidation technique. The major findings are:

(1) The results showed that the degradation as well as the conversion rate of O-cresol is rapid where the equilibrium is reached after 90 min with a percentage of about 84.6% at a temperature of 55 °C and $[H_2O_2]$ = 23.2 mM, then it remains constant.

(2) The influence of pH has shown that in acidic medium. The degraded amount of O-cresol is greater in a strongly acidic medium pH = 2, then it gradually decreased when the solution became neutral and basic.

(3) The formation of 2-methylbenzoquinone increases at the same time as the rise in temperature.

(4) The decrease in the iron content and the increase in the oxygen content present in the catalyst after the catalytic oxidation show that the oxidation process has taken place.

(5) Moreover, the possible modifications of the structural, textural and surface chemistry properties of Mont-Na has been analyzed before and after the catalytic test using several techniques (X-ray diffraction, Fourier transform infrared spectroscopy, N_2 adsorption–desorption isotherm at 77 K, thermo-gravimetric analysis coupled to mass spectroscopy, chemical composition and pH at point of zero charge).

(6) The set of characterization results suggest that this is a catalytic oxidation of O-cresol following degradation to other intermediate hydroxylated organic compounds such as carboxylic acids and the final products H_2O and CO_2.

(7) H_2O_2 oxidation of O-cresol in the presence of local clay proved to be an effective means for the removal and degradation of O-cresol contained in industrial influents.

Acknowledgments

Financial support for this work by the Algerian Directorate General of Scientific Research and Technological Development (DGRSDT) and the Ministry for Higher Education and Scientific Research is gratefully appreciated. The authors would like to thank the staff of Servicios Te´cnicos de Investigacio´n (SSTTI) of the University of Alicante for performing characterization.

References

Abdollahi, Y.; Abdullah, A.H.; Zainal, Z.; Yusof, N. A. (2001) Photodegradation of o-cresol by ZnO under visible light irradiation. *Int. j. adv. res. sci. eng. Technol.,* 8 (2), 135 – 144.

Adan, C.; Carbajo, J.; Bahamonde, A.;–Martinez-Aias, A. (2009) Phenol photodegradation with oxygen and hydrogen peroxide over TiO_2 and Fe-doped TiO_2. *Catal. Today*., **143** (3–4), 247–252.

Adav, S.S.; Chen, M.Y.; Lee, D.J .; N.Q. Ren. (2007) Degradation of phenol by aerobic granules and isolated yeast Candida tropicalis. *Biotechnol. Bioeng*., **96** (5), 844–852.

ATSDR. (2008) *Agency for Toxic Substances and Disease Registry Division of Toxicology and Health Human Sciences* (ATSDR), Cresols - ToxFAQs™, N° CAS 1319-77-33.

Bertella, F .; Pergher, S. B.C. (2015) Pillaring of bentonite clay with Al and Co. *Micropor. Mesopor. Mat*., **201**, 116–123.

Borji, S.H.; Nasseri, S.; Mahvi, A.H.; Nabizadeh, R; Javadi, A.H. (2014) Investigation of photocatalytic degradation of phenol by Fe(III)-doped TiO_2 and TiO_2 nanoparticles. *J. Environ. Health. Sci. Eng*., **12**, 101-110.

Chena, D.; Liua, F.; Zonga, L.; Suna, X.; Zhanga, X.; Zhua, C.; Taoa, X .; Li, A. (2016) Integrated adsorptive technique for efficient recovery of m-cresol and m-toluidine from actual acidic and salty wastewater. *J. Hazard. Mater*., **312**, 192–199.

Deng, Y– .; Englehardt, J. D. (2006) Treatment of landfill leachate by the Fenton process. *Water Res*., **40** (20), 3683– 3694.

Ellias, N; Sugunan, S. (2014) Wet peroxide oxidation of phenol over Cerium impregnated Aluminium and Iron- Aluminium Pillared Clays. *J. Appl. Chem*., **7** (5), 80-85.

Feddal, I.; Ramdani, A.; Taleb, S.; Gaigneaux, E.M.; Batis, N .; N. Ghaffour. (2014) Adsorption capacity of methylene blue, an organic pollutant, by montmorillonite clay *Desalin. Water Treat*., **52** (13-15), 2654–2661.

Gavrilescu, M., Demnerová, K., Aamand, J., Agathos, S and Fava, F. (2015). Emerging pollutants in the environment: present and future challenges in biomonitoring, ecological risks and bioremediation. *New Biotechnology*., **32** (1), 147-156.

Gil, A.; Korili, S. A .; Vicente, M. A. (2008) Recent Advances in the Control and Characterization of the Porous Structure of Pillared Clay Catalysts. *Catal. Rev.*, **50** (2), 153–221.

Hadjar, H.; Hamdi, B.; Ania, C.O. (2011) Adsorption of p-cresol on novel diatomite/carbon composites. *J. Hazard. Mater*., **188** (1-3), 304–310.

Herbache, H .; Ramdani, A.; Maghni, A.; Taleb, Z.; Taleb, S.; Morallon, E.; Brahmi, R. (2016) Removal of o-Cresol from aqueous solution using Algerian Na-Clay as adsorbent. *Desalin. Water Treat*., **57** (43), 20511–20519.

Hernandez-Esparza, M.; Doria-Serrano, M.C.; Acero Salinas, G .; Ruiz-Trevino, F.A. (2006) Removal of high phenol concentrations with adapted activated sludge in suspended form and entrapped in calcium alginate/ cross-linked poly (N-vinyl pyrrolidone) hydrogels. *Biotechnol. Prog*., **22** (6), 1552–1559.

Hocine, O.; Boufatit, M.; Khouider, A. (2004) Use of montmorillonite clays as adsorbents of hazardous pollutants. *Desalination*., **167** (1), 141-145.

Huang, J. (2009). Treatment of phenol and p-cresol in aqueous solution by adsorption using a carbonylated hyper cross linked polymeric adsorbent. *J. Hazard. Mater*., **168** (2-3), 1028–1034.

Jiang, S.; Zhang, H .; Yan, Y. (2015) Catalytic wet peroxide oxidation of phenol wastewater over a novel Cu–ZSM-5 membrane catalyst. *Catal. Commun*., **71**, 28-31.

Kavitha, V .; Palanivelu, K. (2005) Destruction of cresols by Fenton oxidation process. *Water Res*., **39** (13), 3062–3072.

Kausar, A.; Iqbal, M.; Javed, A.; Aftab, K.; Nazli, Z.; Bhatti, H. N .; S. Nouren. (2018) Dyes adsorption using clay and modified clay: A review. *J. Mol. Liq*., **256**, 395–407.

Kennedy, L.J.; Vijaya, J.J.; Sekaran, G.; Kayalvizhi, K. (2007) Equilibrium, kinetic and thermodynamic studies on the adsorption of m-cresol onto micro- and mesoporous carbon. *J. Hazard. Mater*. **149** (1), 134–143.

Khaki, M.R.D.; Shafeeyan, M. S.; Raman, A.A.A .; Daud, W. M. A.W. (2017) Application of doped photocatalysts for organic pollutant degradation - A review. *J. Environ. Manage*., **198** (2), 78-94.

Khunphonoi, R .; Grisdanurak, N. (2016) Mechanism pathway and kinetics of p-cresol photocatalytic degradation over titania nanorods under UV-visible irradiation. *Chem. Eng. J*., **296**, 420-427.

Kurian, M .; Sugunan, S. (2006). Wet peroxide oxidation of phenol over mixed pillared montmorillonites. *Chem. Eng. J*., **115** (3), 139-146.

Lahbabi, N.; Rais, Z.; Hajjaji, M.; Kacim, S. (2009) Oxydation du phenol sur un catalyseur à base de Fer supporté sur une argile marocaine. *Afrique Science*., **5** (3), 14–24.

Lassouane, F.; Amrani, S .; Aït-Amar, H. (2013) Evaluation of o-cresol degradation potential by a strain of Pseudomonas aeruginosa S8. *Desalin. Water. Treat*., **51** (40-42), 7577-7585.

Li, Y.; Hu, X.; Liu, X.; Zhang, Y.; Zhao, Q.; Ning, P .; S. Tian. (2018) Adsorption behavior of phenol by reversible surfactant-modified montmorillonite: Mechanism, thermodynamics, and regeneration. *Chem. Eng., J*. **334**, 1214-1221.

Ling, H.; Kim, K.; Liu, Z.; Shi, J.; Zhu, X .; J. Huang. (2015) Photocatalytic degradation of phenol in water on as-prepared and surface modified TiO_2 nanoparticles. *Catal. Today*., **258** (1), 96-102.

Madejova, J. (2003) FTIR techniques in clay mineral studies review. *Vib. Spectrosc*., **31** (1), 1–10.

Mohan, D .; Pittman, C.U. (2007) Arsenic removal from water/wastewater using adsorbents-a critical review. *J. Hazard. Mater*., **142** (1-2), 1–53.

Molina, C.B.; Casas, J.A.; Zazo, J.A .; Rodriguez, J.J. (2006) A comparison of Al-Fe and Zr-Fe pillared clays for catalytic wet peroxide oxidation. *Chem. Eng. J*., **118** (1-2), 29–35.

Navalon, S.; Alvaro, M .; Garcia, H. (2010) Heterogeneous Fenton catalysts based on clays, silicas and zeolites. *App. Catal. B. Environ*., **99** (1-2), 1–26.

Official Journal of the Algerian Republic N°41. (2012) Standards for physicochemical parameters of treated wastewater for agriculture. Algiers, Algeria.

Ourari, A.; Tennah, F.; Ruíz-Rosas, R.; Aggoun, D.; Morallón, E. (2018) Bentonite Modified Carbon Paste Electrode as a Selective Electrochemical Sensor for the Detection of Cadmium and Lead in Aqueous Solution. *Int. J. Electrochem. Sci*. **13**, 1683 – 1699.

Ramdani, A.; Taleb, S.; Benghalem, A.; Deratani, A .; Ghaffour, N. (2015) Enhancement of Saharan groundwater quality by reducing its fluoride concentration using different materials. *Desalin. Water Treat*., **54** (1), 3444–3453.

Ren, Y.; Peng, L.; Zhao, G .; Wei, C. (2014). Degradation of mcresol via the ortho cleavage pathway by Citrobacter farmeri SC01. *Biochem. Eng. J*., **88**, 108–114.

Saiah, O.; Hachemaoui, A .;Yahiaoui, A. (2017) Synthesis of a Conducting Nanocomposite by Intercalative Copolymerisation of Furan and Aniline in Montmorillonite. *Int. Polym. Proc*., **32** (4), 515-518.

Salazar-Gil, K.; Díaz-Nava, M.C .; Solache-Ríos, M. (2016) Removal of red 2 and yellow 6 by Zn- and-Na modified zeolitic tuffs in the presence of H_2O_2. *Desalin. Water Treat.,* **57** (35), 16626-16632.

Sennour, R.; Mimane, G.; Benghalem, A .; Taleb, S. (2009) Removal of the persistent pollutant chlorobenzene by adsorption onto activated montmorillonite. *Appl. Clay Sci*., **43** (3-4), 503–506.

Shadnia, H.; Wright, J.S. (2008) Understanding the toxicity of phenols: using quantitative structure- activity relationship and enthalpy changes to discriminate between possible mechanisms. *Chem. Res. Toxicol*., **21** (6), 1197–1204.

Shahrezaei, F.; Mansouri, Y.; Zinatizadeh, A.A. L–.; Akhbari, A. (2012) Process modeling and kinetic evaluation of petroleum refinery wastewater treatment in a photocatalytic reactor using TiO2 nanoparticles. *Powder Technol*., **221**, 203–212.

Shivaraman, N.; Pandey, R. (2000) Characterization and biodegradation of phenolic wastewater. *J. Indian Assoc. Environ*. *Manage*., **27**, 12–15.

Tabué Youmbi, J. G.; Feumba, R.; Njitat, V.T.; Marsily, G- .; Ekodeck, G.E. (2013) Water pollution and health risks at Yaoundé, Cameroon. *C.R.BIOL*., **336** (5-6), 310–316.

Taleb, Z.; Montilla, F.; Quijada,C.; Morallon, E.; Taleb. S. (2014) Electrochemical and In Situ FTIR Study of o-Cresol on Platinum Electrode in Acid Medium. *Electrocatalysis.*, **5** (2), 186–192.

Titus, E.; Kalkar, A.K-.; Gaikar, V.G. (2002) Adsorption of anilines and cresols on NaX and different cation exchanged zeolites (equilibrium, kinetic, and IR investigations). *Sep. Sci. Technol*., **37** (1), 105–125.

Toh, R.H.; Lim, P.E.; Seng, C.E.; R. Adnan. (2013) Immobilized acclimated biomass-powdered activated carbon for the bioregeneration of granular activated carbon loaded with phenol and o-cresol, Bioresour. *Bioresour. Technol*., **143**, 265–274.

Valsania, M.C.; Fasano, F.; Richardson, S.D .; Vincenti, M. (2012) Investigation of the degradation of cresols in the treatments with ozone. *Water Res*., **46** (8), 2795-2804.

Vijayakumar, J.; Chikkala, S.K.; Mandal, S .; Mayadevi, S. (2011) Adsorption of cresols on zinc-aluminium hydroxides—A comparison with zeolite-X. *Sep. Sci. Technol.* **46** (3), 483–488.

Wang, Y.; Wei, H.; Liu, P.; Yu, Y.; Zhao, Y.; Li, X.; Jiang, W.; Wang, J.; Yang, X.; Sun, C. (2015). Effect of structural defects on activated carbon catalysts in catalytic wet peroxide oxidation of m-cresol. *Catal.Today*., **258** (1), 120–131.

Wernert, V.; Schaf, O.; Faure, V.; Brunet, P.; Doub, L.; Berland, Y.; Boulet, P.; Kuchta, B .; R. Denoye. (2006) Adsorption of the uremic toxin p-cresol onto hemodialysis membranes and microporous adsorbent zeolite silicalite. *J. Biotechnol*., **123** (2), 164–173.

William, L .; Roper, M.D. (1992) *Agency for Toxic Substances and Disease Registry,* Toxicological profile for cresols, U.S. Public Health Service.

Yan, Y.; Wu, X .; Zhang, H. (2016) Catalytic wet peroxide oxidation of phenol over Fe_2O_3/MCM-41 in a fixed bed reactor. *Sep. Sci. Technol*., **171**, 52–61.

Yi, S.; Zhuang, W.Q.; Wu, B.; Tay, S.T.L .; Tay, J.H. (2006) Biodegradation of p-nitrophenol by aerobic granules in a sequencing batch reactor. *Environ. Sci. Technol*., **40** (7), 2396–2401.

Zaviska, F.; Drogui, P.; Mercier, G–.; Blais, J.F. (2009) Advanced oxidation processes in water treatment and industrial effluent: Application to the degradation of refractory pollutants. *Rev. Water. Sci*. **22** (1), 535–564.

List of Tables

Table 1-Mont-Na Fluorescence X Before and after catalytic oxidation

Table 2-BET specific surface area values of Mont-Na before and after adsorption and oxidation of O-cresol experiments

Figures captions

Figure 1- Effect of the initial H_2O_2 concentration on the O-cresol degradation. [O-cresol]: 62.5 mg/L. Catalyst weight: 15 mg. Temperature: 25 °C. pH= 7, Contact time:150 min.

Figure 2-Effect of temperature on the catalytic oxidation of O-cresol. [O-cresol]: 62.5 mg/L. [H_2O_2] = 23.2 Mm. Catalyst weight:15 mg. pH= 7. Contact time: 150 min.

Figure 3-Kinetics of the catalytic oxidation of o-cresol at different temperatures. The evolution of the conversion is plotted as a function of the reaction time. [O-cresol]: 62.5 mg/L. [H_2O_2]: 23.2 mM. Catalyst weight: 15 mg. pH= 7.

Figure 4- Effect of pH on the catalytic oxidation of o-cresol. [O-cresol]: 62.5 mg/L. [H_2O_2] = 23.2 Mm. Catalyst weight:15 mg. Contact time: 150 min.

Figure 5- Evolution of the degradation of O-cresol and the formation of 2-methylbenzoquinone as a function of the reaction time (O-Cresol λmax = 270 nm, 2-methylbenzoquinone λmax = 250 nm). [O-cresol]: 62.5 mg/L. [H_2O_2]: 23.2 mM. Catalyst weight: 60 mg.

Figure 6- Evolution of the pH of the reaction medium during the catalytic degradation of O-cresol supported by Mont-Na. [O-cresol]: 62.5 mg/L. [H_2O_2]: 23.2 mM. Catalyst weight: 60 mg.

Figure 7- Catalytic oxidation of O-Cresol supported by Mont-Na.

Figure 8- X-Ray Diffractogram of Mont-Na, Mont-A and Mont-AO samples.

Figure 9- FT-IR spectra of Mont-Na, Mont-A and Mont-AO samples.

Figure 10-Thermogravimetric analysis of Mont-Na sample.

Figure 11-Thermogravimetric analysis of the Mont-Na sample after O-cresol adsorption.

Figure 12- DTA/ TGA profile of oxidation of O-cresol-Mont-Na.

Figure 13- DTA/MS analysis of Mont-A and Mont-AO samples under atm He and atm air.

Table 1

Element (%)	O	Si	Al	Mg	K	Fe	Na
Mont-Na	48.9	29.9	12.5	1.94	0.869	2.04	3.29
Mont-AO	49.6	32.9	9.85	2.18	1.66	1.62	1.38

Table 2

Samples	Mont-Na	Mont-A	Mont-AO
S_{BET} (m^2/g)	67	43	40
Volume of micropores (cm^3/g)	0.04	0.08	0.06
Pore diameter (Å)	406	547	510

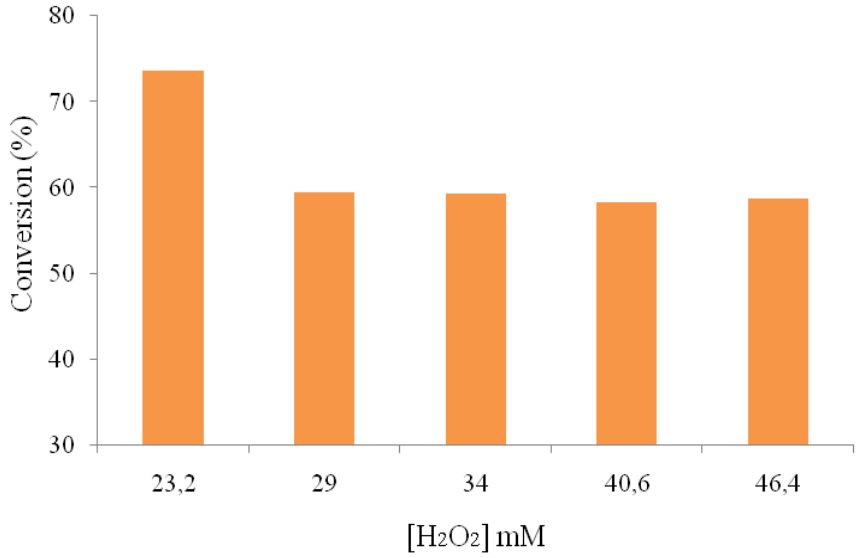

Figure 1

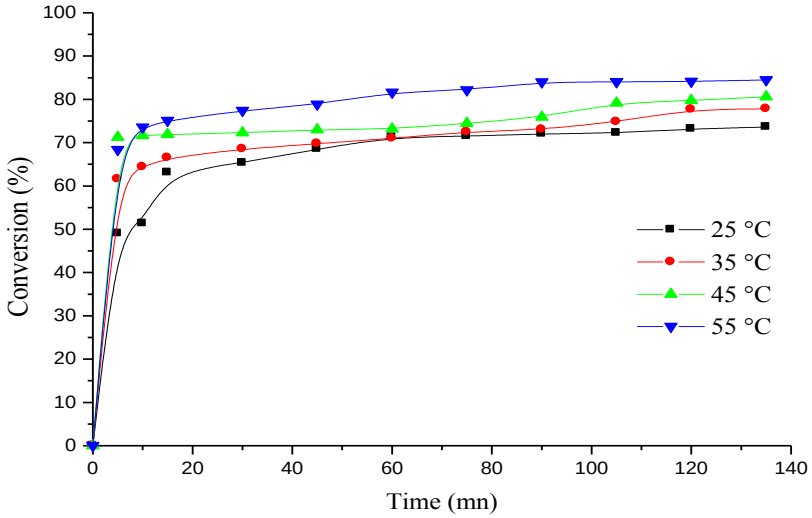

Figure 2

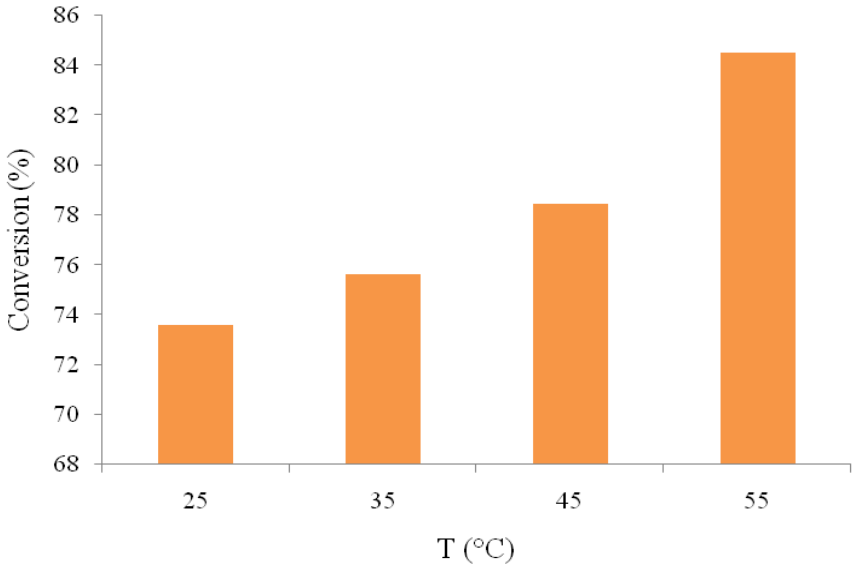

Figure 3

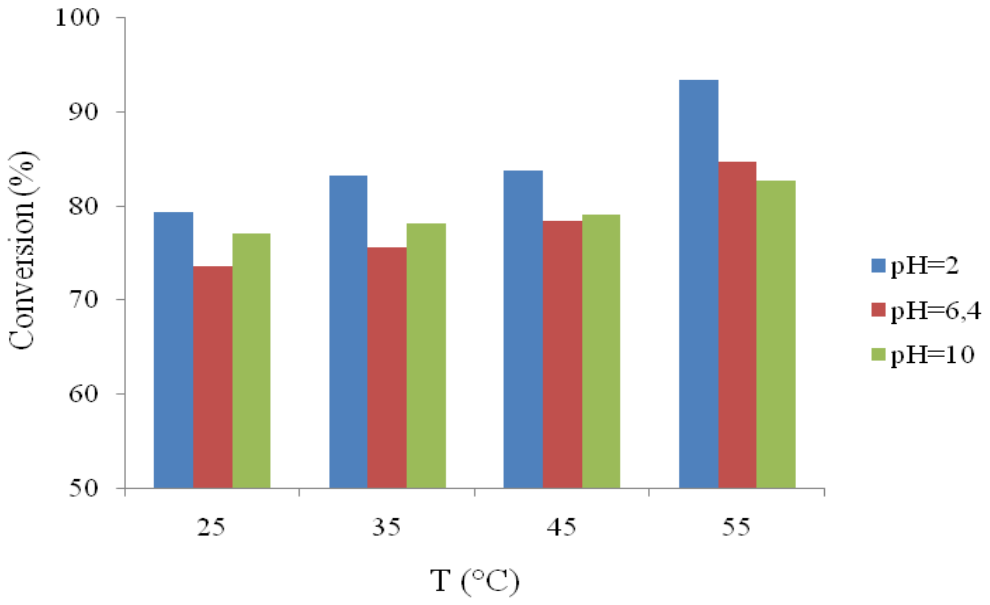

Figure 4

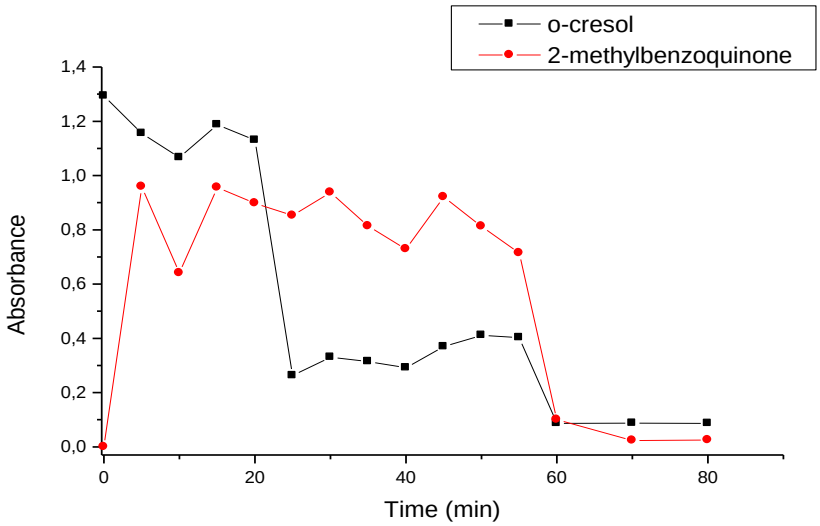

Figure 5

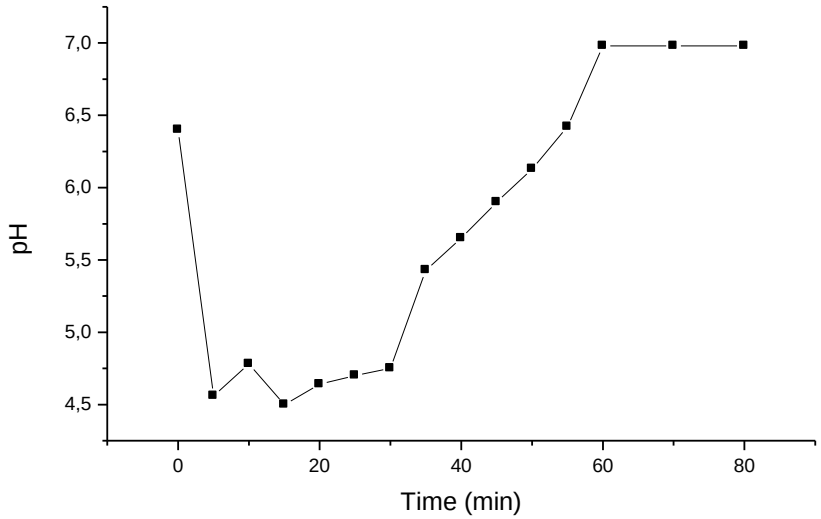

Figure 6

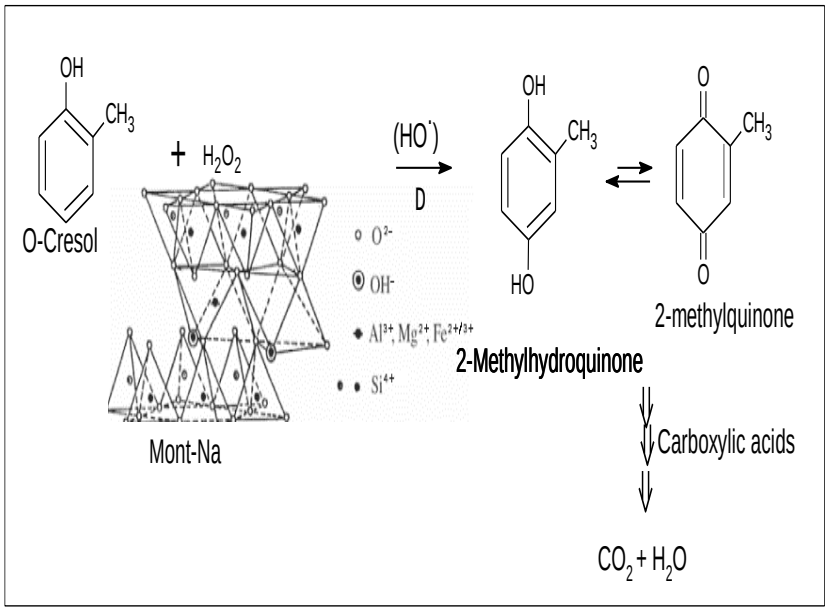

Figure 7

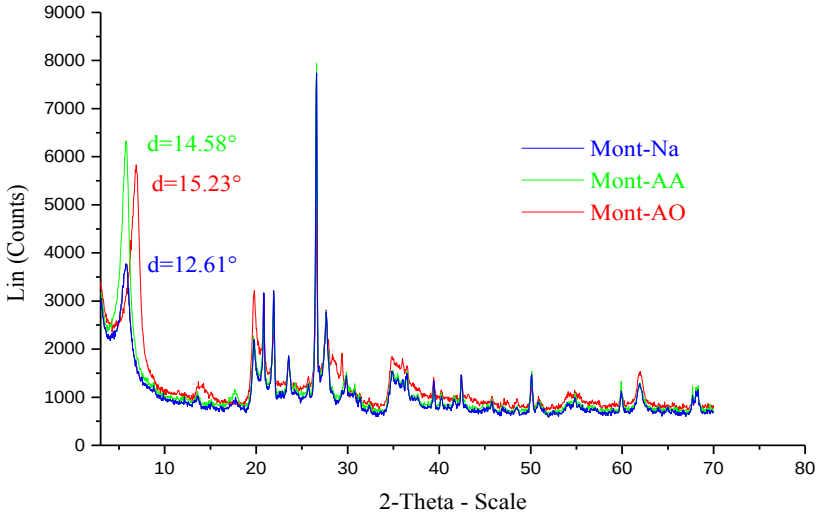

Figure 8

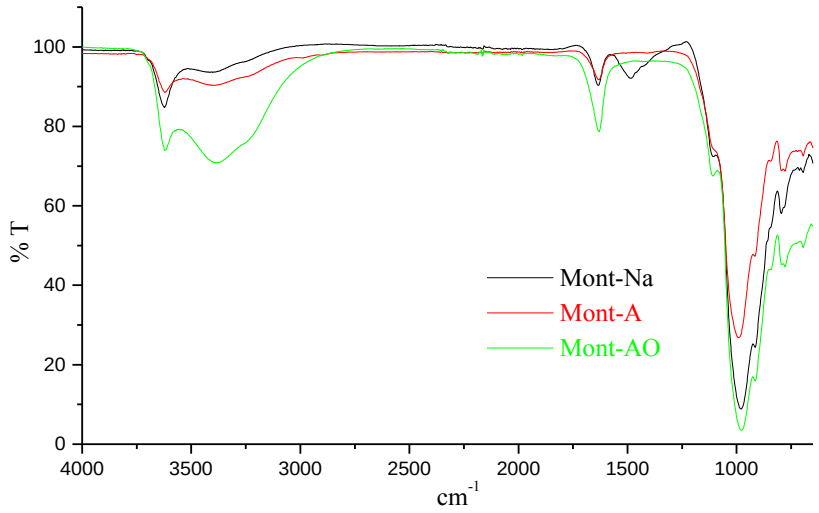

Figure 9

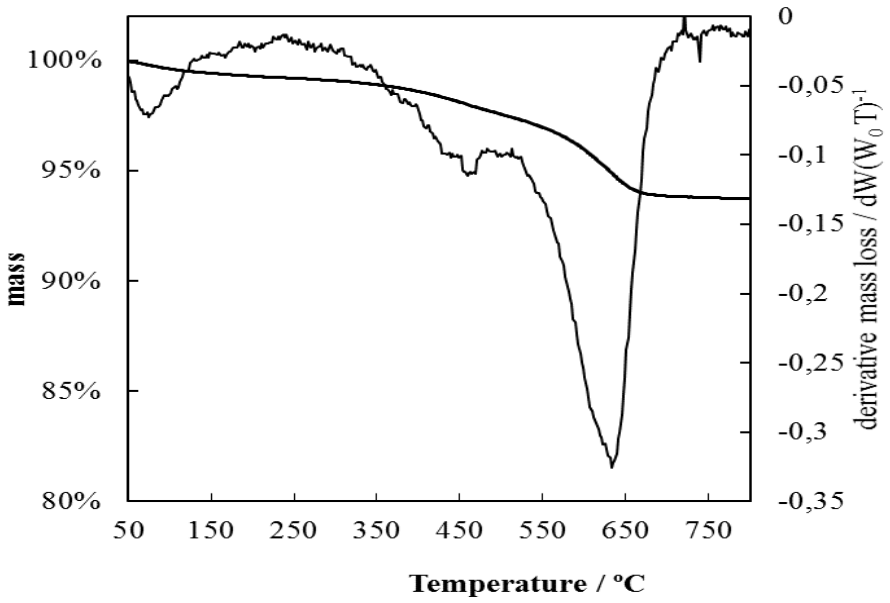

Figure 10

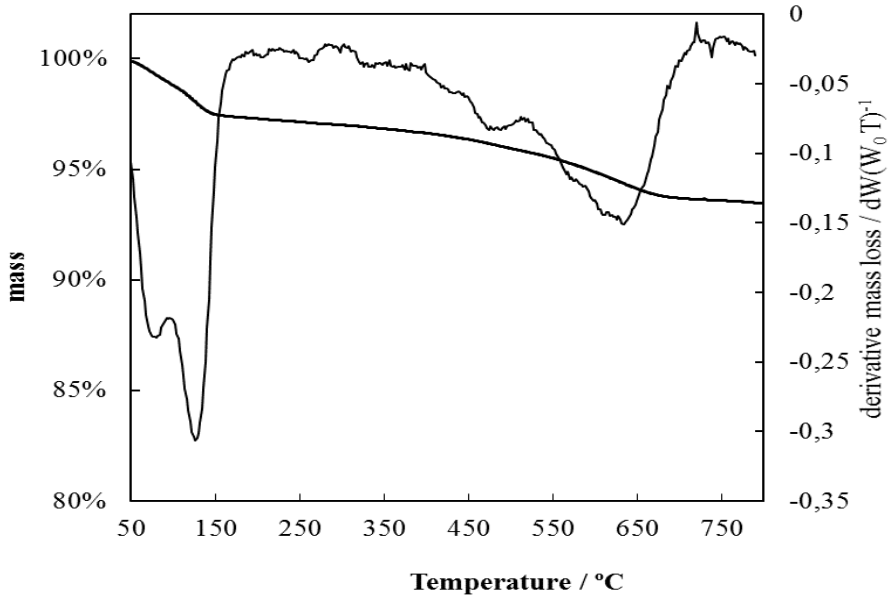

Figure 11

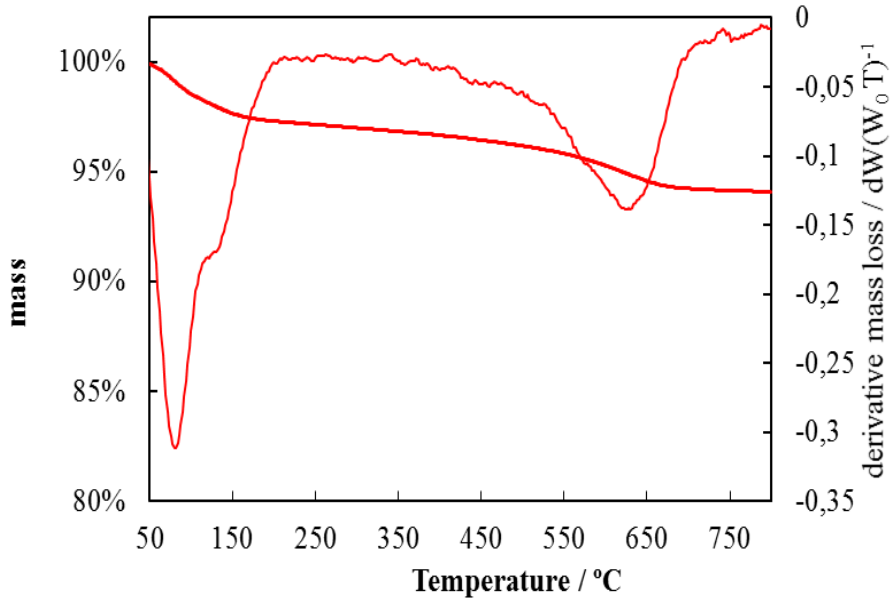

Figure 12

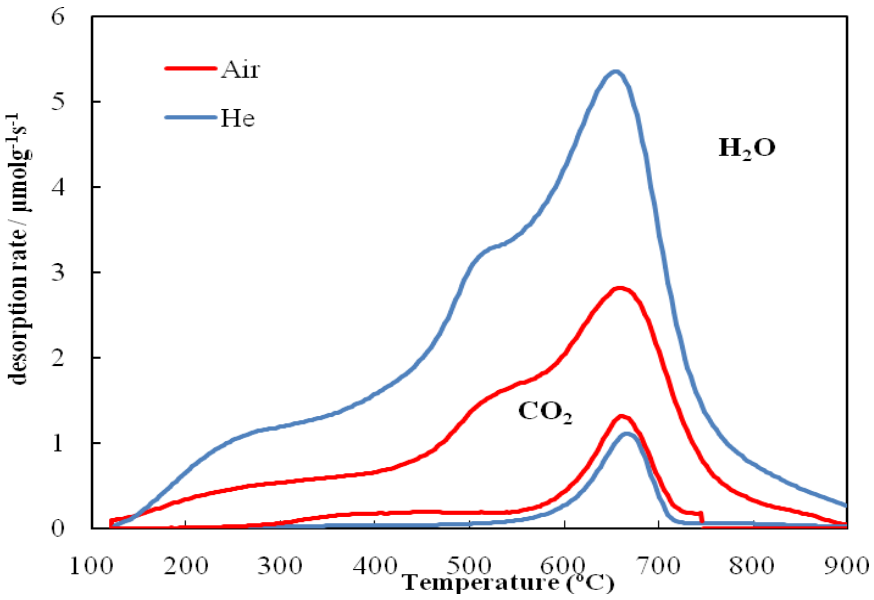

Figure 13